

Supporting Information For:

Electrochemical Synthesis of Core-Shell Nanoparticles by Seed-Mediated Selective Deposition

Joon Ho Park^a, Seon-Mi Jin^b, Eunji Lee^b and Hyun S. Ahn^{a,*}

^aContribution from Department of Chemistry, Yonsei University, 50 Yonsei-ro, Seodaemun-gu, Seoul, 03722 Republic of Korea

^bSchool of Materials Science and Engineering, Gwangju Institute of Science and Technology (GIST), 123 Cheomdangwagi-ro, Bukgu, Gwangju, Republic of Korea, eunjilee@gist.ac.kr

Email: ahnhs@yonsei.ac.kr

Table of Contents	Page
Experimental	S2
Linear Sweep Voltammograms of 100 mM Co ²⁺ , Ni ²⁺ , Fe ²⁺ , Cu ²⁺ Ions (Figure S1)	S4
TEM and Elemental Mapping Images of AnD synthesized Au Nanoparticles (Figure S2)	S5
TEM and Elemental Mapping Images of Au-Ni Nanoparticles with Smaller and Larger Sizes (Figure S3)	S6
Estimation of Au Core Nanoparticle Density	S7
Synthetic Chronoamperograms During Shell Deposition (Figure S4)	S8
TEM/HAADF-STEM Images of Core-shell Nanoparticles and Their FFT Images (Figure S5)	S9
Metal ratios of Nanoparticles Measured by Elemental Mapping (Table S1)	S10
TEM Images and EDX Mapping Images of Polycrystalline Au-Cu Nanoparticles (Figure S6)	S11
TEM Images and Linear Sweep Voltammograms as a Result of 100 mM Cr ³⁺ , Mn ²⁺ Reduction (Figure S7)	S12
TEM Images and Elemental Line Scan of Au-Co Nanoparticles with Varying Thickness (Figure S8)	S13
TEM Images and Elemental Line Scan of Au-Fe Nanoparticles with Varying Thickness (Figure S9)	S14
TEM Images of Au-Cu Nanoparticles of Various Deposition Charges (Figure S10)	S15
TEM Tomographic Reconstruction and 3D Images of Au-Ni Nanoparticles (Figure S11)	S16
Linear Sweep Voltammograms of Nanoparticle Decorated TEM grids and Glassy Carbon Electrodes in Their OER (Figure S12)	S17
Cyclic Voltammograms of Au-Fe Decorated Electrode in OER Relevant Potential Ranges (Figure S13)	S18
ICP-OES Measurement of Metal Contents in Nanoparticle Decorated Electrodes (Table S2)	S19
TEM and Elemental Mapping Images of Au-Co Nanoparticles after Extended OER Operation (Figure S14)	S20
Cyclic Voltammograms of Au-Co Decorated Electrode before and after Continued OER Catalysis (Figure S15)	S21
Oxygen Evolution Reaction Catalysis Tafel Plots of Catalyst Electrodes (Figure S16)	S22
Linear Sweep Voltammograms of Au-Ni and 100 nm Ni nanoparticle decorated electrodes (Figure S17)	S23
SEM Images and Elemental Mapping Images of Au-Ni Decorated Glassy Carbon Plate (Figure S18)	S24
References	S25

Experimental

General

Deionized water was prepared using Youngin Instruments Aquapuri 5 water purification system (18.2 M Ω -cm, 3 ppb total oxidizable carbon). Chloroform (CHCl₃, HPLC grade) and Tetrabutylammonium perchlorate (TBAP, $\geq 98.0\%$) were obtained from TCI. Platinum on graphitized carbon (Pt/C, 20 wt% loading), Dioctyl sulfosuccinate sodium salt (AOT, $\geq 97\%$), sodium perchlorate monohydrate (NaClO₄·H₂O, 98%), Nafion solution (5 wt% in lower aliphatic alcohols and water, water content 15–20%) were purchased from Sigma-Aldrich and used as received. Cobalt (II) sulfate heptahydrate (CoSO₄·7H₂O, $\geq 99\%$), nickel (II) sulfate hexahydrate (NiSO₄·6H₂O, $\geq 98\%$), and iron (II) sulfate heptahydrate (FeSO₄·7H₂O $\geq 99\%$) were purchased from Sigma-Aldrich and used as received. Anhydrous Copper (II) sulfate (CuSO₄) was obtained from Sigma-Aldrich. Gold (III) chloride hydrate (HAuCl₄·xH₂O $\geq 99.99\%$) was obtained from Sigma-Aldrich, kept in a dark storage box. Nickel nanoparticle (100 nm, $\geq 99\%$) was purchased from Sigma-Aldrich and used as received. Iridium Oxide (IrO₂) was purchased from Alfa-Aesar and used as received. TEM grids with pure carbon on nickel grids were purchased from Ted Pella, Inc. All electrochemical measurements were conducted using a CH Instruments (Austin, TX) model 760e potentiostat. A JEM-F200 TEM were operated to obtain the TEM/HAADF-STEM data and an Oxford Instruments energy dispersive x-ray spectroscopy (EDX) detector was used to obtain the EDX elemental mapping and line scan data. Agilent 7900 ICP-MS was operated to obtain ICP-OES data.

Aqueous nanoDroplet (AnD) synthesis

AnD synthesis procedure was similar to that in our previous report.^{S1} Water saturated chloroform solution (5 mL) containing 1 mM AOT was mixed with 100 μ L of aqueous solution containing 0.2 M NaClO₄ and 10 mM HAuCl₄. The solution was vortexed for 20 s and then horn sonicated for 20 cycles in pulse (3 s on, 7 s off for each cycle) to generate AnDs dispersed in a chloroform continuous phase. The AnD solution was stored in an ice bath.

Core-shell nanoparticle synthesis by AnD electrolysis and selective electrodeposition

A small amount (typically 49 pM AnD concentration in the reaction cell) of AnD solution was injected into chloroform containing 0.2 M TBAP, in a custom designed PTFE cell, employing TEM grids as working electrodes. A limited area of the TEM grid was exposed (1.2 mm diameter) to the solution in order to maximize S/N ratio and to be able to directly monitor AnD electrochemistry *in-situ* (see Figure 1b and Figure S2 for example). Ag/AgNO₃ and Pt wire were used as reference and counter electrodes, respectively. Total solution volume was controlled between 600 and 650 μ L for all synthesis experiments. The working electrode was held at a potential bias of -0.4 V. After Au nanoparticle deposition by AnD electrolysis, the TEM grid was rinsed with acetone and dried for 2 h. Then, for shell deposition, 0.1 M metal (FeSO₄, CoSO₄, NiSO₄) aqueous solution containing 0.5 M H₃BO₃ and 0.1 M K₂SO₄ was injected in the PTFE cell. The solutions were adjusted to pH 3 with H₂SO₄. For Cu deposition, 0.1 M CuSO₄ aqueous solution containing 0.1 M K₂SO₄ was used. At this stage, the counter electrode was Pt wire and the reference electrode was replaced by Ag/AgCl. The potential was applied from -0.55 V to -0.7 V (vs. RHE) and current collected by chronoamperometry until the metal ions (Fe²⁺, Ni²⁺, Co²⁺) reduced by 0.375 C/cm², 0.75 C/cm² and 1.5 C/cm². For Cu deposition, the working electrode was held at a potential bias in range of 0.95 V to 0.7 V by 0.0375 C/cm².

Oxygen evolution reaction (OER) catalysis

To prepare working electrodes, the amount of all metals was controlled to *ca.* 0.1 mg/cm². 100 mg of Pt/C was dispersed in mixed solvent of 8 mL deionized water, 2 mL isopropanol and 40 μ L Nafion solution and ultrasonicated for 30 min. Then 10 μ L (100 μ g Pt/C, 20 μ g Pt; for a Pt loading density of 0.102 mg/cm²) of the dispersion solution was drop-casted on a 5 mm (diameter) glassy carbon disk electrode, dried for 4 h. For IrO₂ electrode, 22 mg of IrO₂ was dispersed in a solution of the same composition as Pt/C and ultrasonicated for 30 min. Then 10 μ L (22 μ g IrO₂; for a Ir loading density of 0.096 mg/cm²) of the dispersion solution was drop-casted on the 5 mm (diameter) glassy carbon disk electrode, dried for 4 h. For 100 nm Ni nanoparticle electrode, 10 mg of Ni was dispersed in a solution of the same composition as Pt/C and ultrasonicated for 30 min. Then 7 μ L (7 μ g Ni; for a Ni loading density of 0.099 mg/cm²) of the dispersion solution was drop-casted on the 3 mm (diameter) glassy carbon disk electrode, dried for 2 h. To compare catalysts, Au nanoparticles were electrochemically deposited on a 3 mm glassy carbon disk electrode and 2 cm² glassy carbon plate for 1500 s. After Au nanoparticle deposition, electrochemical shell deposition was performed by the same amount per unit area, similar to the experiment on TEM grid. The catalyst electrode was carefully rinsed with deionized water and dried for 3 h in air. All the oxygen evolution catalysis experiments were progressed in N₂ saturated 1 M KOH solution. A Pt wire was used as a counter electrode and a Hg/HgO reference electrode was employed.

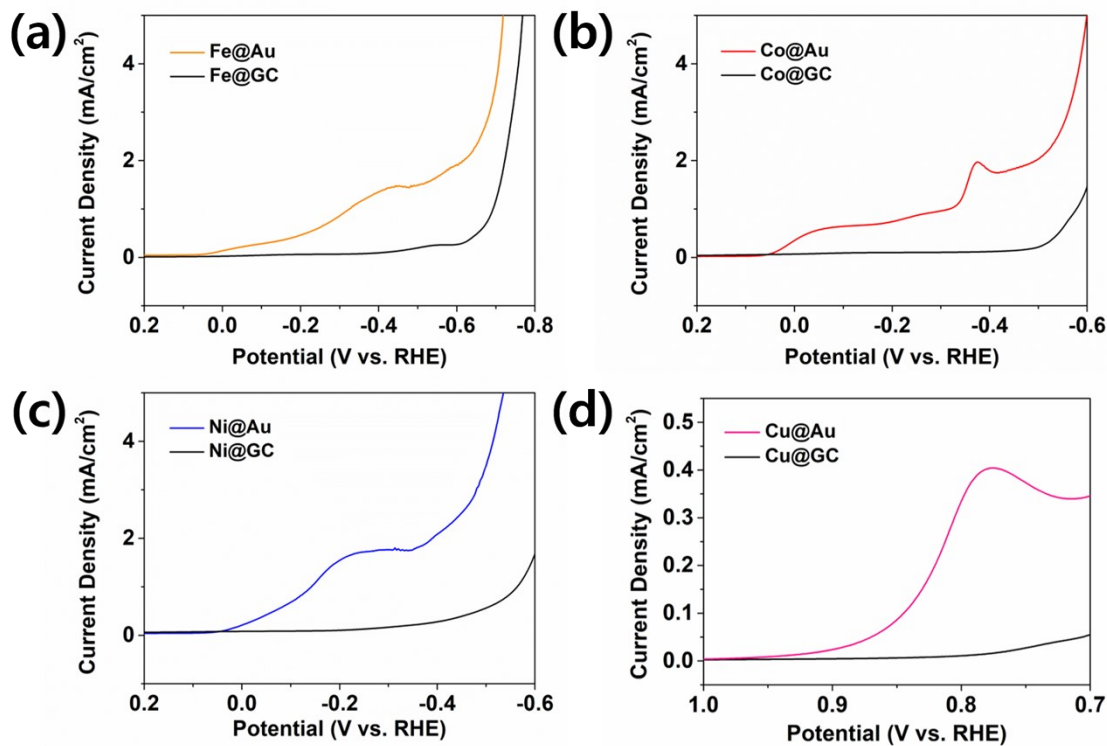


Figure S1. Linear sweep voltammograms (LSVs) corresponding to the reduction of 100 mM (a) FeSO₄, (b) CoSO₄, (c) NiSO₄, (d) CuSO₄ obtained at a 2 mm gold disk electrode and a 3 mm glassy carbon disk electrode in N₂ saturated aqueous solution. The potential of selective electrodeposition was established in the range in which metal ions were reduced only at the Au electrode.

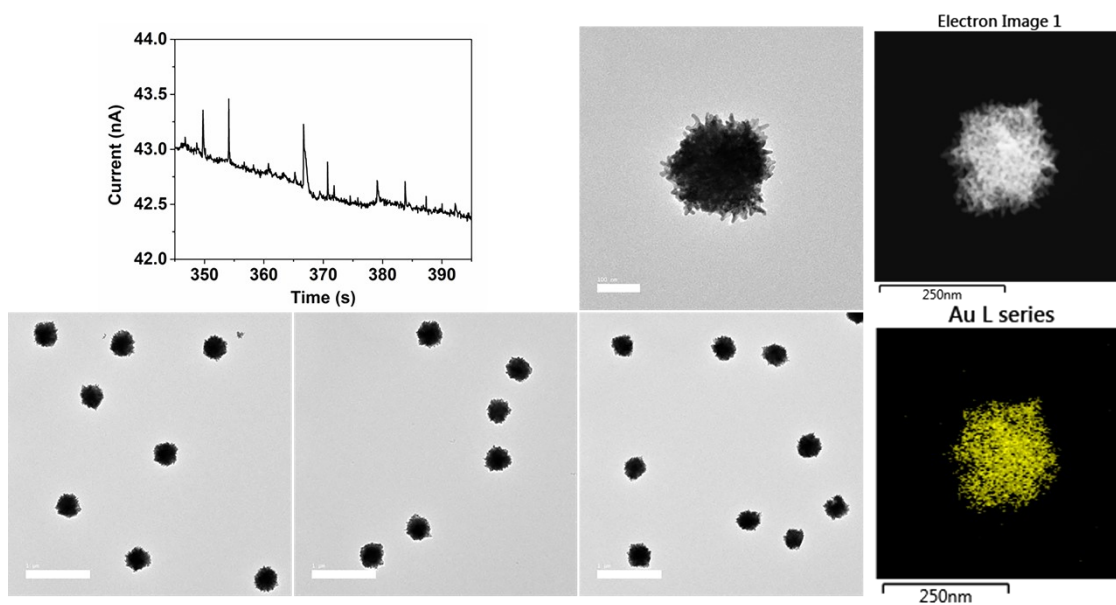


Figure S2. TEM and elemental mapping images of AnD synthesized Au nanoparticles. The Au nanoparticles with size of 210 ± 20 nm are evenly distributed. Each nanoparticle synthesis by the AnD collision and electrolysis events can be monitored in-situ through amperometry.

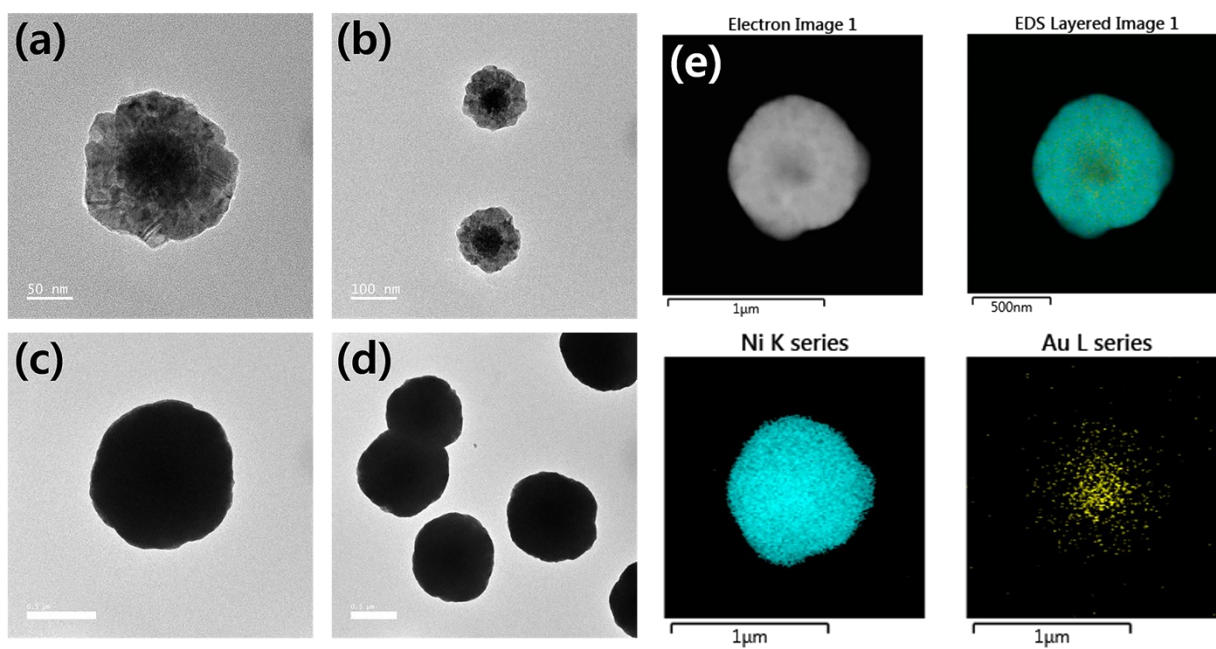


Figure S3. TEM and elemental mapping images of Au-Ni particles for demonstration of ease of nanoparticle dimension control. Particles with smaller size (50 nm core and 25 nm shell) are in image (a) and (b), and those with larger size (400 nm core and 300 nm core) are in image (c) and (d). (e) Elemental mapping of larger particles for identification of the core.

Estimation of Au Core Nanoparticle Density

Electrode collision frequency can be calculated by estimating the diffusion coefficient of the AnDs in solution, the concentration of AnD, and the size of the electrode. For 600 nm diameter aqueous droplets, the frequency is

$$D_{AnD} = \frac{k_B T}{6\pi\eta r_{AnD}}$$

$$D_{AnD} = \frac{(1.381 \times 10^{-23} \text{ kg} \cdot \text{m}^2 \cdot \text{s}^{-2} \cdot \text{K}^{-1}) \times (298 \text{ K})}{6\pi \times (5.36 \times 10^{-4} \text{ kg} \cdot \text{m}^{-1} \cdot \text{s}^{-1}) \times (3.00 \times 10^{-7} \text{ m})} = \frac{\text{m}^2}{\text{s}}$$

$$C_{AnD} = 4.9 \times 10^{-11} \text{ M} = 49 \text{ pM}$$

$$f_{AnD} = 4D_{AnD}C_{AnD}r_{elec}N_A$$

$$f_{AnD} = 4 \times (1.36 \times 10^{-12} \text{ m}^2 \cdot \text{s}^{-1}) \times (0.49 \times 10^{-7} \text{ mol} \cdot \text{m}^{-3}) \times (6.0221 \times 10^{23} \text{ mol}^{-1}) = 104.5 \text{ s}^{-1}$$

Nanomaterial-electrode collision frequencies generally can be predicted with good accuracies when employing small electrodes as reported, but at larger electrodes with linear diffusion region, the prediction increasingly becomes inaccurate.^{S2,S3} The frequency in experiment is lower than that from calculations by a factor of 10 or greater typically, so the number of gold nanoparticles is expected to be less than that calculated.

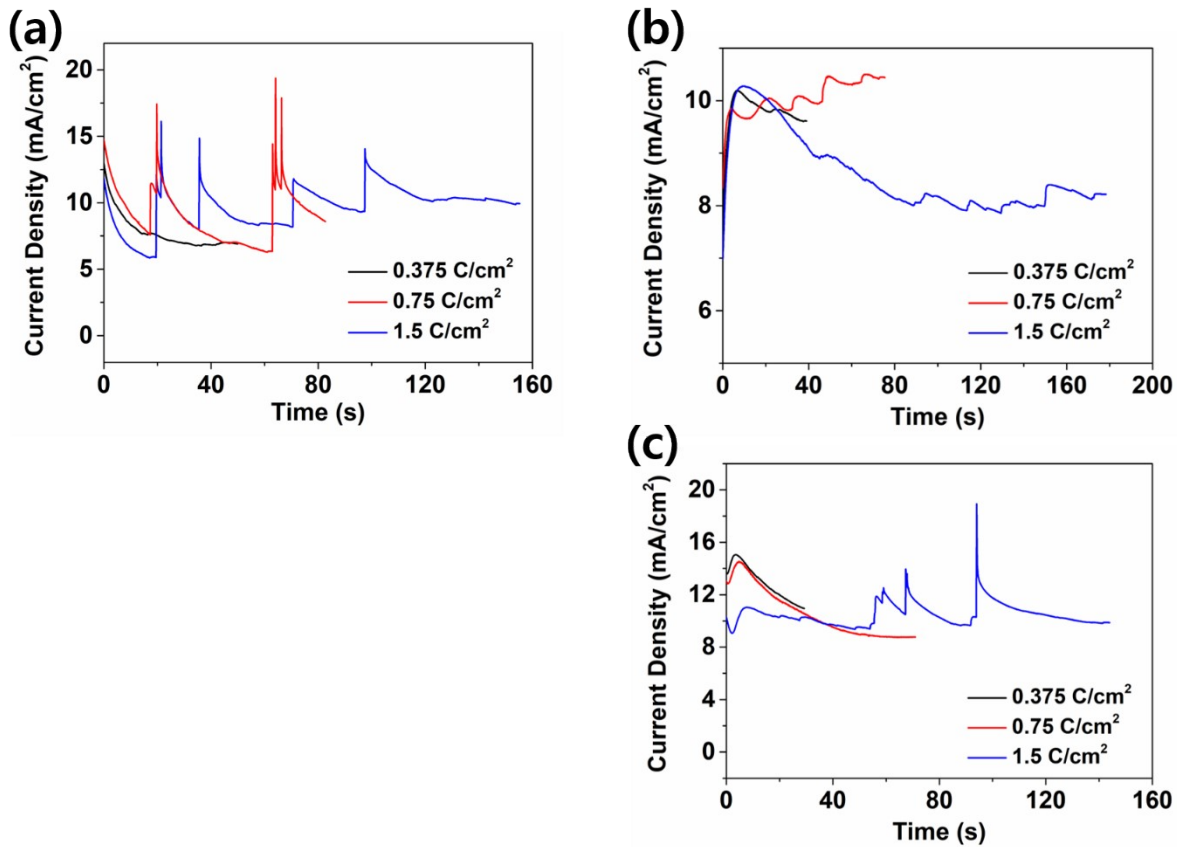


Figure S4. Chronoamperograms corresponding to the shell deposition process for (a) Au-Fe, (b) Au-Co, (c) Au-Fe. The passed charge during deposition was controlled by 0.375 C/cm², 0.75 C/cm², and 1.5 C/cm². The sudden spikes in the current were due to occasional convection generated by pipetting action of the deposition bath, in order to remove small hydrogen bubbles on the electrode formed via HER.

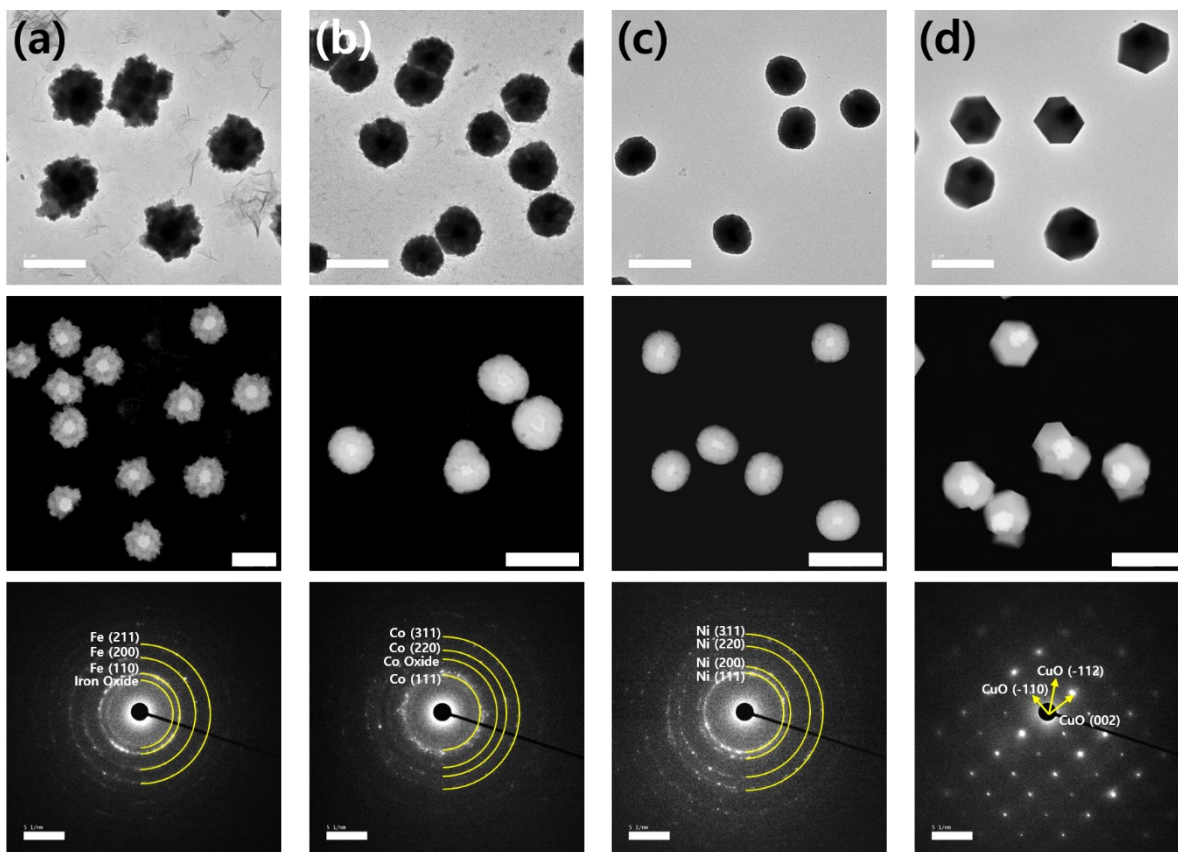


Figure S5. TEM/HAADF-STEM images of core-shell nanoparticles and their FFT images of **(a)** Au-Fe, **(b)** Au-Co, **(c)** Au-Ni, **(d)** Au-Cu core-shell nanoparticles. The gold nanoparticles constitute the cores and the 1st-row transition metal shells cover around them. Selected area electron diffraction (SAED) exhibiting ring patterns confirm the polycrystalline structures except for Au-Cu. The SAED pattern for Au-Cu exhibits single crystalline oxide phase, demonstrating severe level of oxidation of Cu shell. The scale bars are 1 μm .

Table S1. Metal ratios of nanoparticles measured by elemental mapping.

Element	Au-Fe	Au-Co	Au-Ni	Au-Cu
O	20.03	18.79	12.48	27.43
Fe / Co / Ni / Cu	75.60	78.06	80.03	69.6
Au	4.37	3.14	7.49	2.97

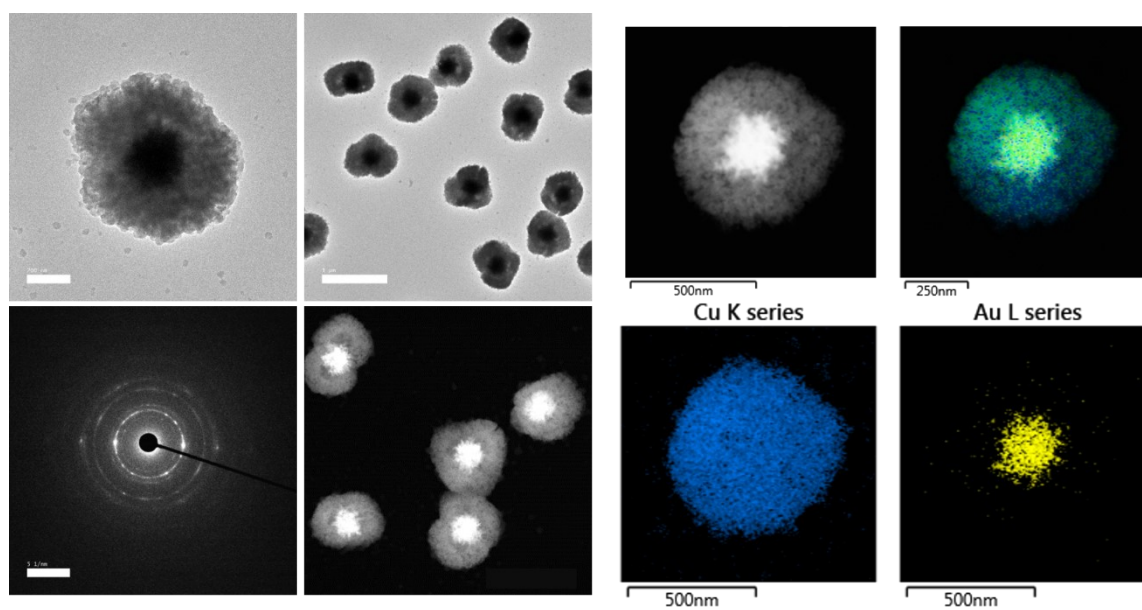


Figure S6. TEM and EDX mapping images of polycrystalline Au-Cu nanoparticles. In low potential range, the Cu shell was constructed polycrystalline as exhibited in its electron diffraction pattern.

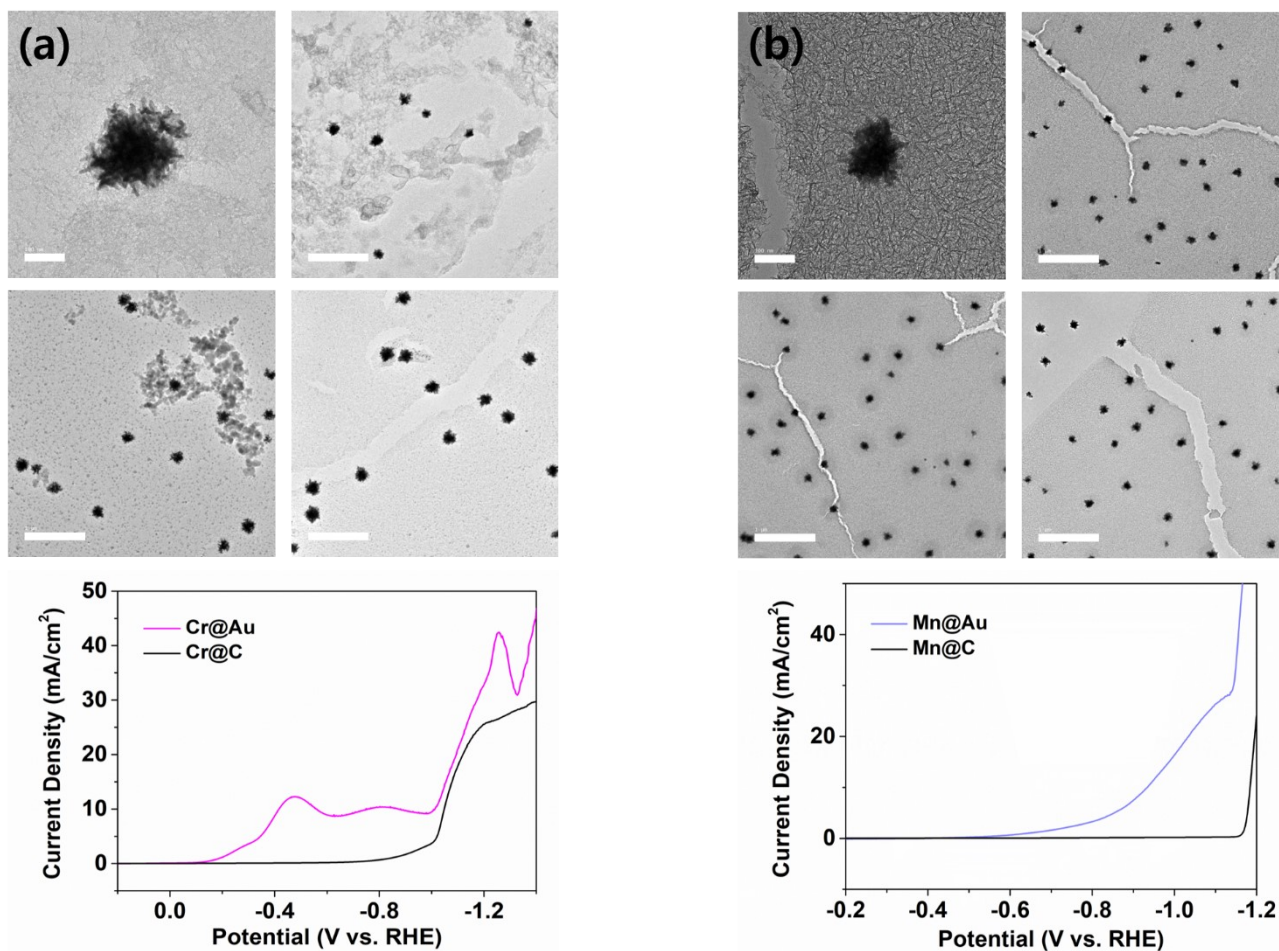


Figure S7. TEM images and linear sweep voltammograms as a result of 100 mM Cr^{3+} , Mn^{2+} reduction at a 2 mm gold disk electrode and 3mm glassy carbon disk electrode in N_2 saturated aqueous solution. When Cr^{3+} and Mn^{2+} are reduced to Cr and Mn, HER has already progressed considerably, therefore the shells were not formed clearly as other metals, but rather sheets of oxyhydroxides were produced.

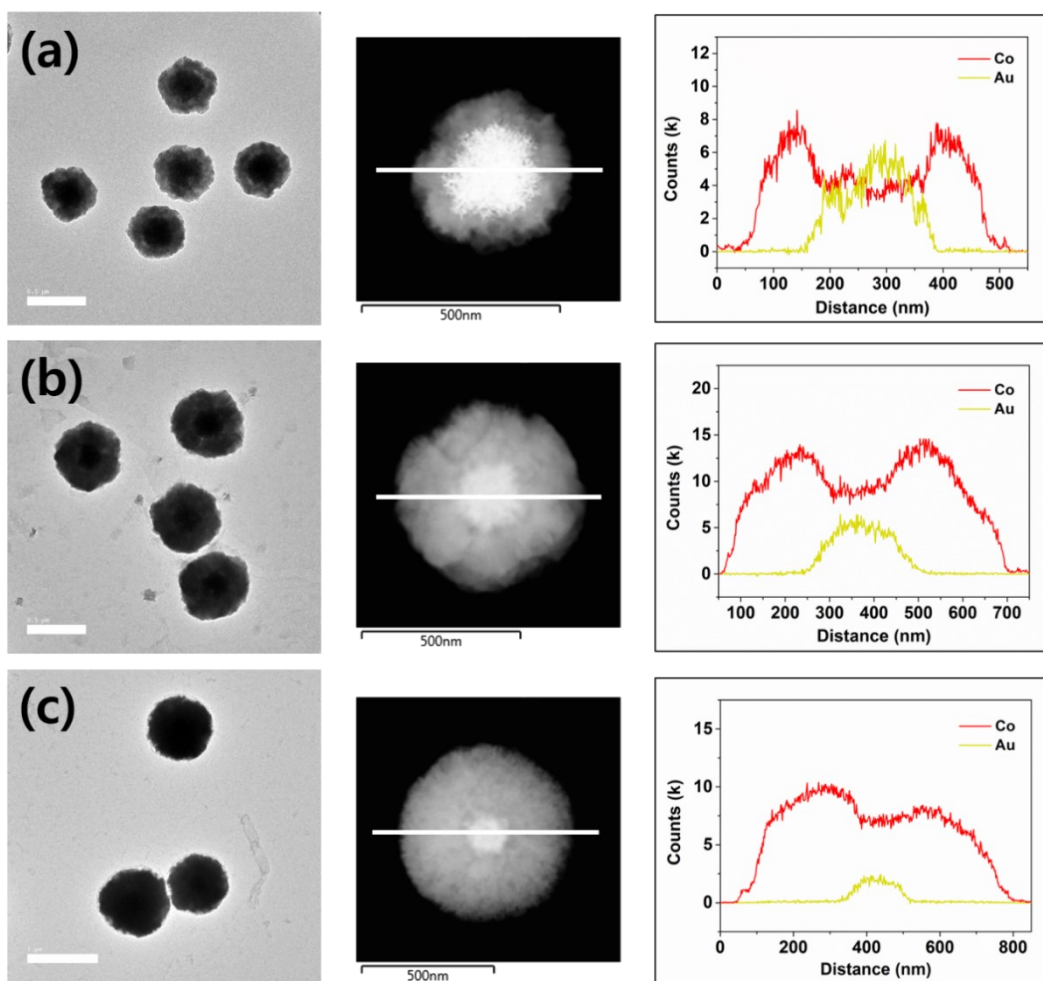


Figure S8. TEM Images and elemental line scan of Au-Co nanoparticles with varying thickness: **(a)** 0.375 C/cm^2 **(b)** 0.75 C/cm^2 **(c)** 1.5 C/cm^2 . Results from the data set are culminated in Figure 3.

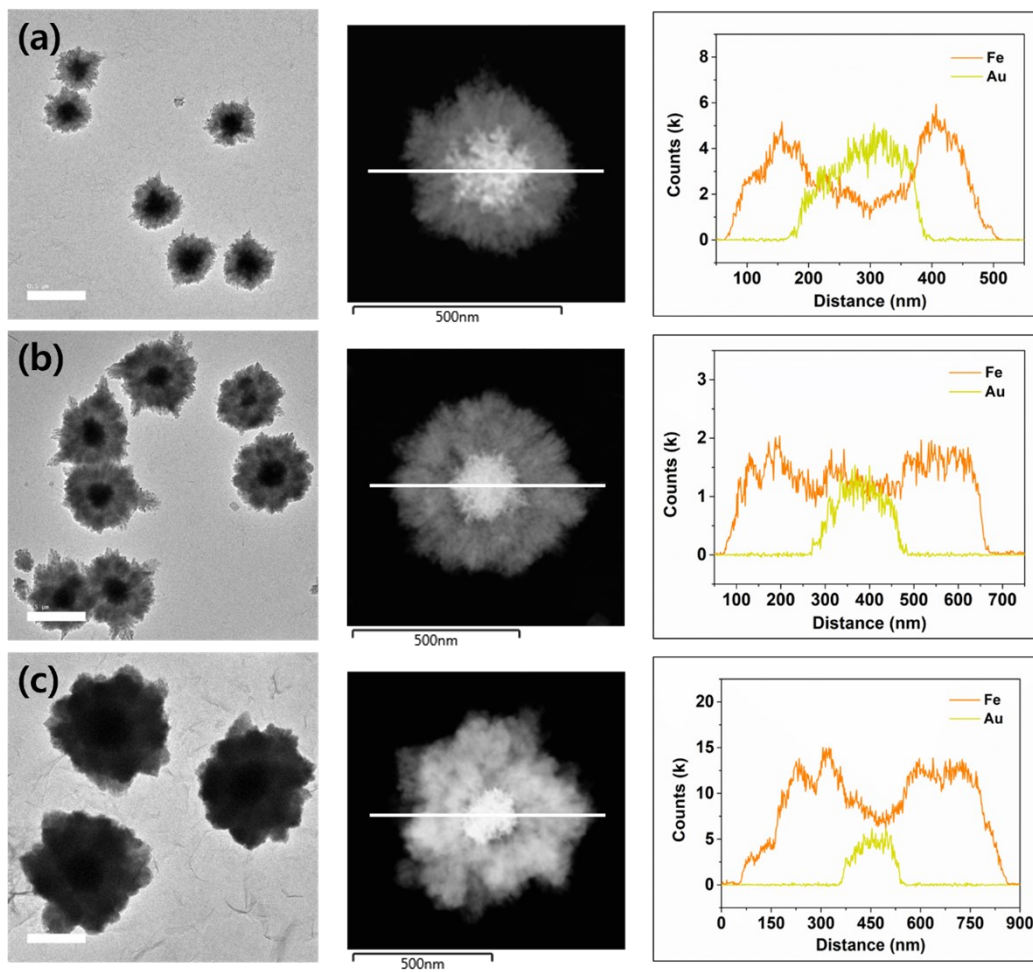
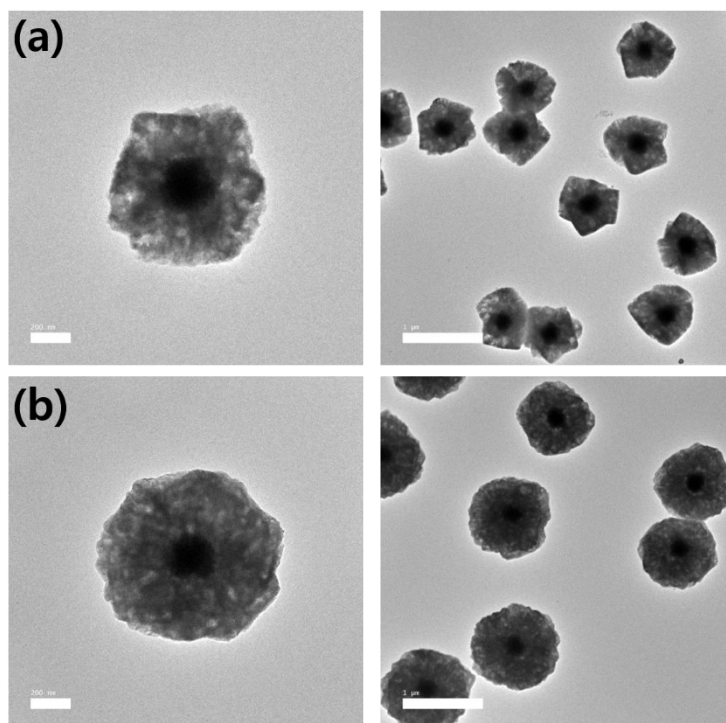


Figure S9. TEM images and elemental line scan of Au-Fe nanoparticles with varying thickness: **(a)** 0.375 C/cm² **(b)** 0.75 C/cm² **(c)** 1.5 C/cm². Results from the data set are culminated in Figure 3.

Figure S10. TEM images of Au-Cu nanoparticles of various deposition charges: **(a)** 0.0375 C/cm^2 , **(b)** 1.5 C/cm^2 . Cu shell thickness was controllable by control of passed charge during deposition in the same way as Fe, Co, Ni shell deposition.



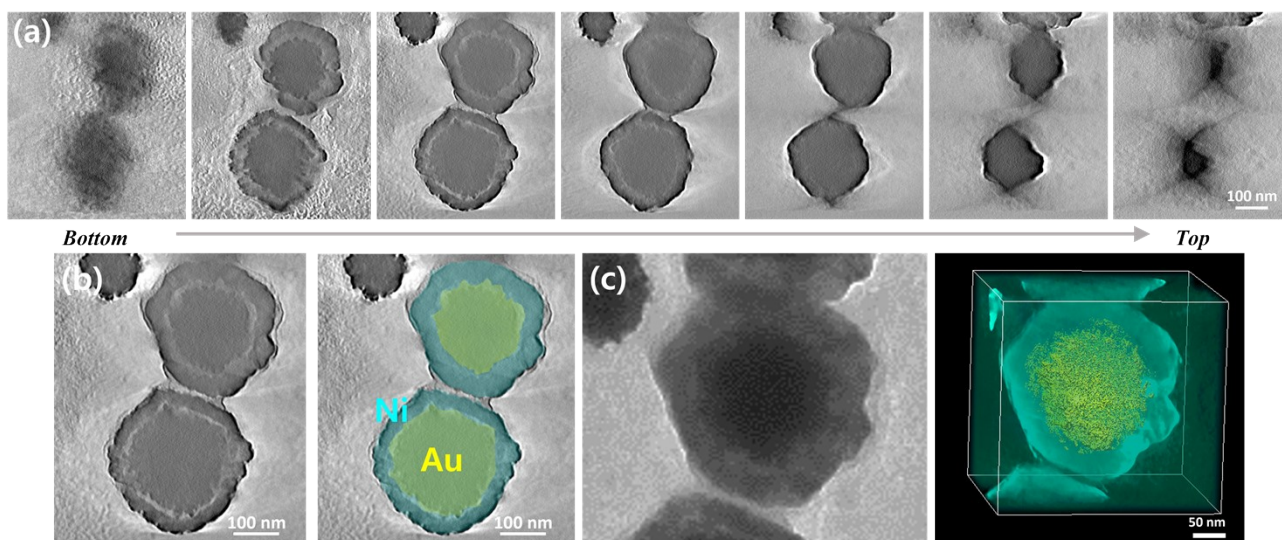


Figure S11. (a) TEM n -xy slice images of 0.375 C/cm^2 level Au-Ni nanoparticles obtained from tomographic reconstruction. The intervals in z -direction between consecutive slices are 35.7 nm . (b) Elemental map of Au-Ni nanoparticles from reconstruction image. (c) TEM image of a Au-Ni nanoparticle and its 3D tomographic image.

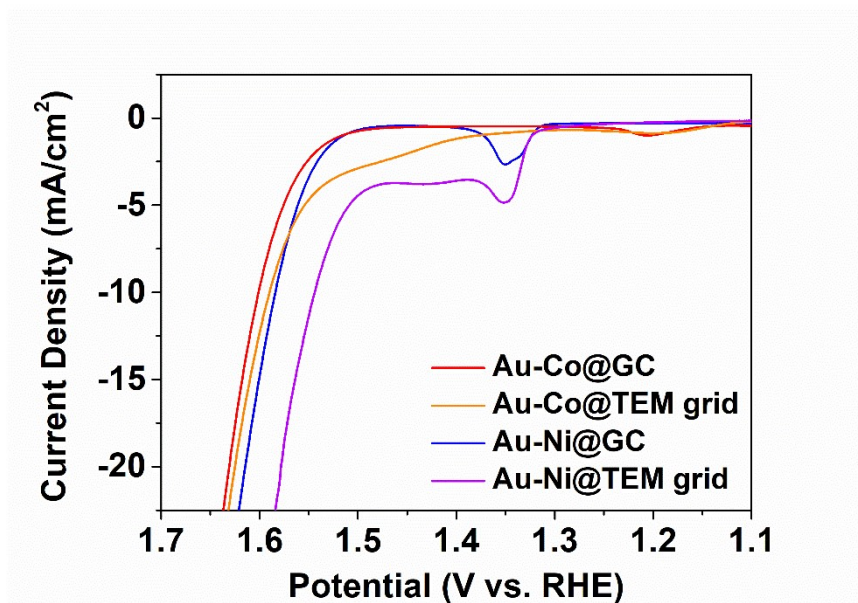


Figure S12. Linear sweep voltammograms of nanoparticle decorated electrodes in their OER. When area normalized, similar behavior is observed without any resistance when compared to catalyst decorated GC.

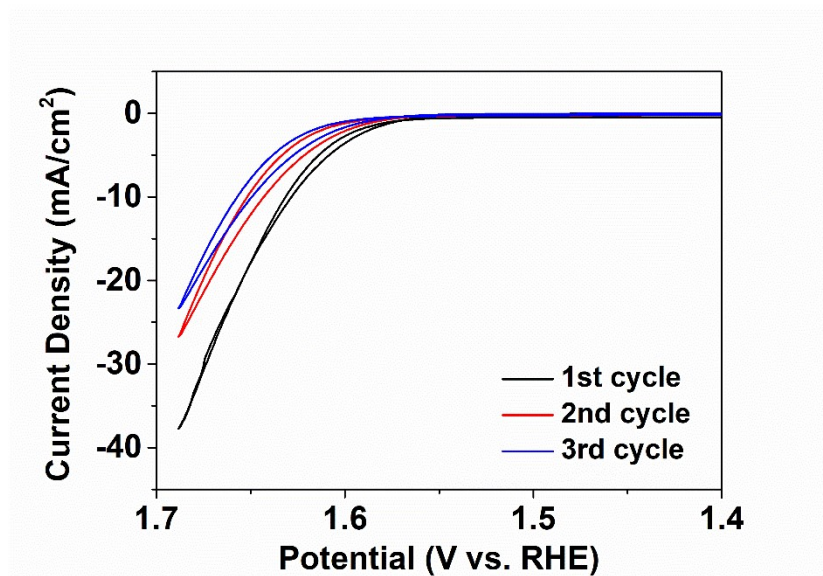


Figure S13. Cyclic voltammograms of Au-Fe decorated electrode in OER relevant potential ranges. At the Au-Fe electrode, the OER current decreases severely in every cycle at CV before continued operation of OER catalysis.

Table S2. ICP-OES measurement of metal contents in nanoparticle decorated electrodes.

	Fe	Co	Ni
Sample Name	Mass [ng]	Mass [ng]	Mass [ng]
Au-Fe	2148	0	0
Au-Co	6	6436	7
Au-Ni	0	1.2	7365

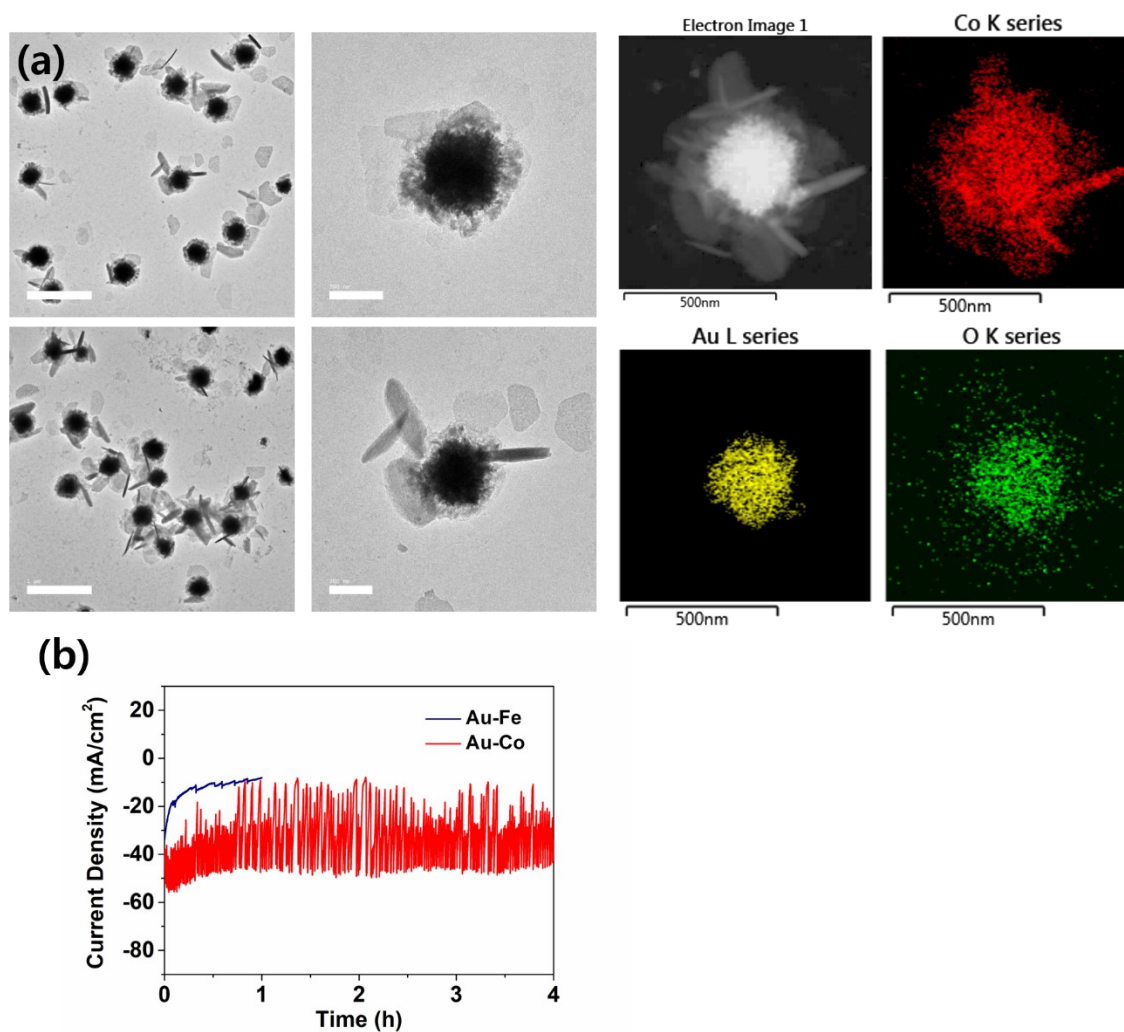


Figure S14. (a) TEM and elemental mapping images of Au-Co nanoparticles after extended OER operation. Significant degradation was confirmed after OER catalysis in contrast to Au-Ni. (b) Chronoamperogram obtained while operating the OER stability experiment for four hours. The working electrode was held at a potential bias of 1.7 V (vs. RHE) for Au-Fe, and 1.65 V for Au-Co. Au-Co has noise due to periodic pipetting to remove evolved oxygen bubbles, but the overall current was maintained. The stability test for Au-Fe was progressed for one hour since a severe current decay was observed.

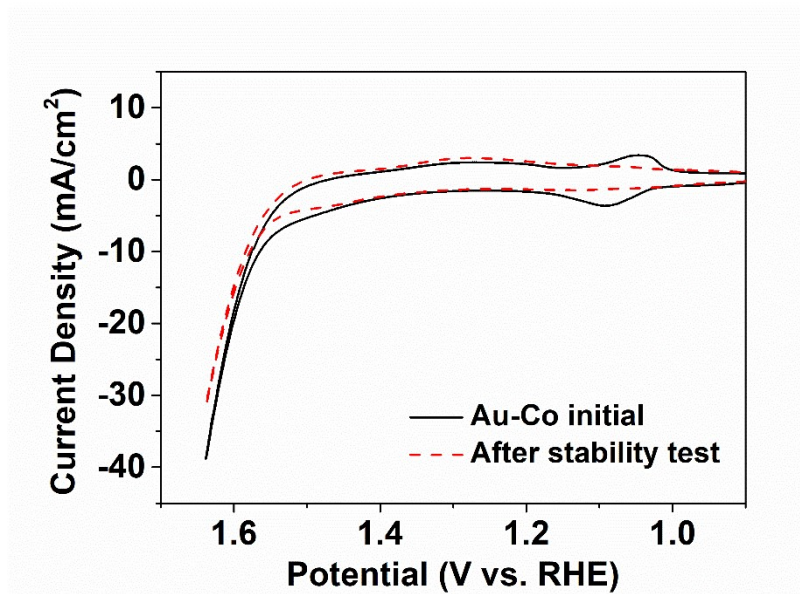


Figure S15. Cyclic voltammograms of Au-Co decorated electrode before and after continued OER catalysis. The decrease in current is not clear in the chronoamperogram, whereas the decay is more apparent in the CV, requiring *ca.* 30 mV overpotential compared to initial catalyst electrode. The typical redox peak of hydroxide to oxyhydroxide transition also significantly decreased in size after catalysis.

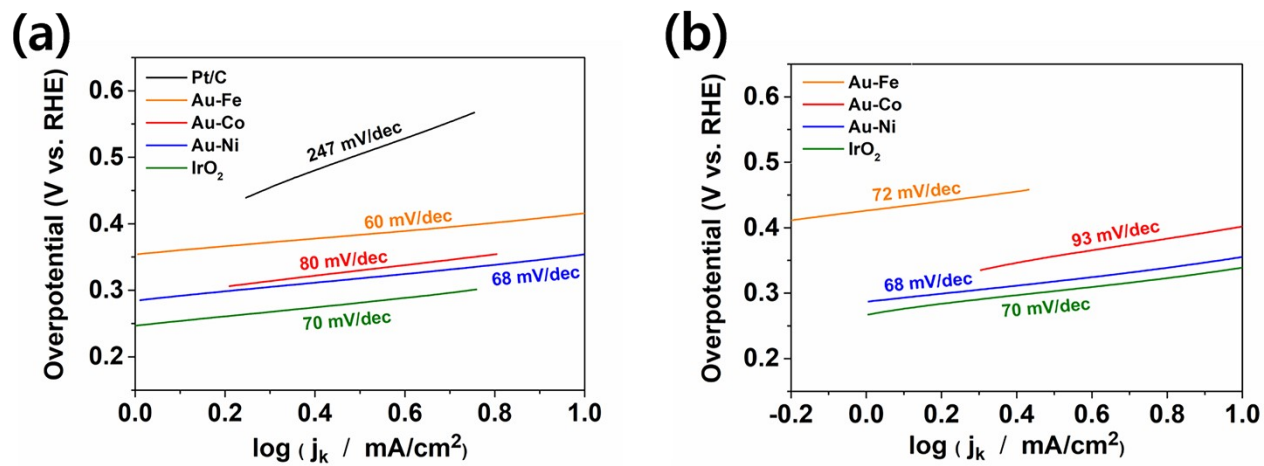


Figure S16. Oxygen evolution catalysis Tafel plots of catalyst electrodes (a) before and (b) after durability test, suggesting similar OER mechanism of Au-Ni and IrO₂.

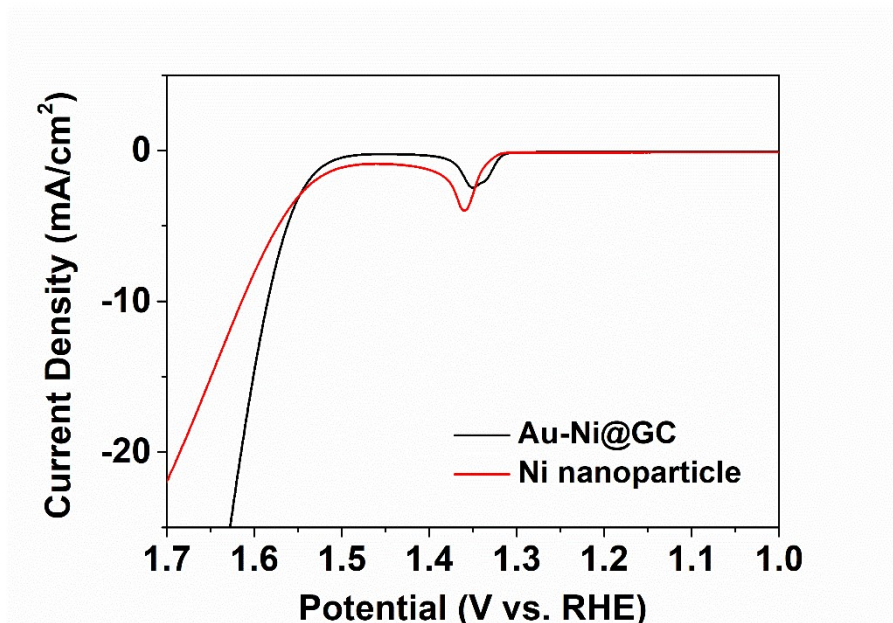


Figure S17. Linear sweep voltammograms of 0.375 C/cm² level Au-Ni and commercial 100 nm Ni nanoparticle decorated 3 mm GC disk electrode comparing the OER catalysis. Despite smaller size of the commercial Ni particles, superior OER catalysis of Au-Ni was demonstrated.

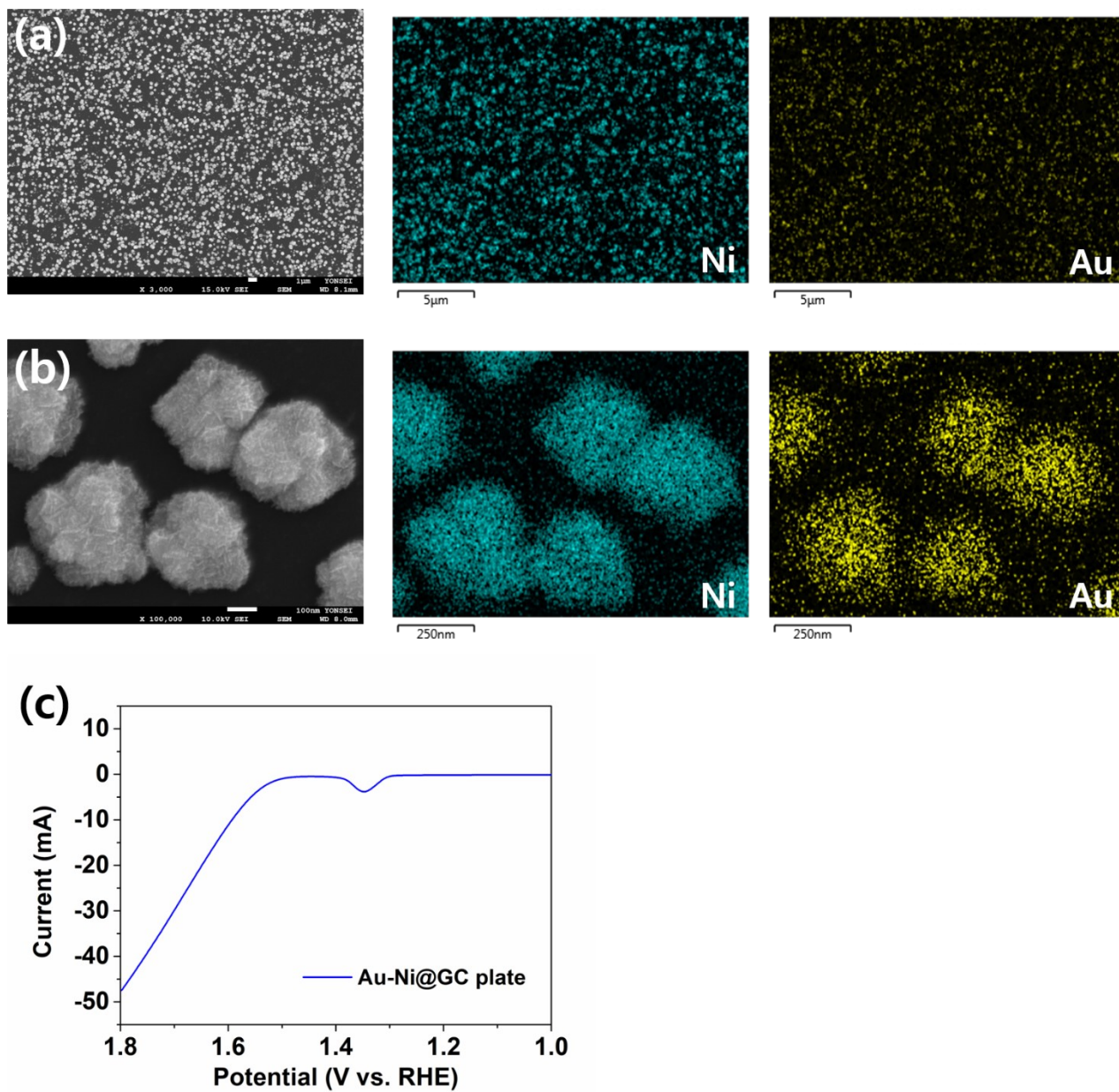


Figure S18. SEM and elemental map images of 0.375 C/cm^2 level Au-Ni decorated glassy carbon plate at (a) low and (b) high magnifications. Nanoparticles with identical size and compositions to those on TEM grids were synthesized. (c) Linear sweep voltammogram of Au-Ni catalyst GC plate in its OER. The scale bars are $1 \mu\text{m}$ in (a) and 100 nm in image (b).

References

- (1) Y. E. Jeun, B. Baek, M. Y. Lee and H. S. Ahn, *Chem. Commun.*, 2018, **54**, 10052-10055.
- (2) H. S. Ahn and A. J. Bard, *Angew. Chem. Int. Ed.*, 2015, **54**, 13753-13757.
- (3) B.-K. Kim, J. Kim and A. J. Bard, *J. Am. Chem. Soc.*, 2015, **137**, 2343–2349.
- (4) T. T. H. Hoang and A. A. Gewirth, *ACS Catal.*, 2016, **6**, 1159–1164.